Functional Materials 11, No.3 (2004) © 2004 — Institute for Single Crystals

Scanning near-field optical microscopy of magnetic structures in magnetic films

V.I.Belotelov, A.S.Logginov, A.V.Nikolaev, A.P.Pyatakov, A.K.Zvezdin[*]

M.Lomonosov Moscow State University, Faculty of Physics, Physics of Oscillations Department, Vorobievy gory, 119991 Moscow, Russia
[*]Institute of General Physics, Russian Academy of Sciences, 38 Vavilov St., 119992 Moscow, Russia

Magnetooptical observation of magnetic domain walls in iron-garnet films by scanning near field optical microscopy has been studied to reveal the advantages of the near-field imaging in terms of spatial resolution. Recent experiments have shown that in case of 5 to 10 μm thick magnetic films, near field observation of domain structures does not provide obvious spatial resolution increase as compared to the conventional optical microscopy. Theoretical analysis based on the Green functions method revealed that the film thickness plays a crucial role in this effect. Qualitative explanation of the resolution deterioration with the increasing film thickness is also given.

Магнитооптическое наблюдение границ магнитных доменов в пленках железных гранатов способом ближне-полевой сканирующей оптической микроскопии исследовано с точки зрения обнаружения преимуществ ближне-полевого изображения в отношении пространственного разрешения. Последние эксперименты показали, что ближне-полевое исследование доменной структуры магнитных пленок толщиной 5–10 мкм не обеспечивает существенного повышения пространственного разрешения по сравнению с обычной оптической микроскопией. Теоретический анализ на основе функций Грина показывает, что решающую роль в этом эффекте играет толщина пленки. Представлено также качественное объяснение ухудшения разрешения с увеличением толщины пленки.

Detailed study of the magnetization distributions on submicrometer spatial scales and the elaboration of corresponding high-resolution techniques is today among the most important problems in applied and fundamental micromagnetism. In the past decade, a significant progress has been made in the development of methods for studying micro- and nanostructures due to appearance and development of magnetic force microscopy which is a version of scanning probe microscopy [1]. Currently, the magnetic force microscopy is characterized by the best spatial resolution in studying magnetic microstructures (tens of nanometers [2]). However, its application leads to a number of problems: difficulties in interpretation and identification of images, an uncontrollable influence of the microprobe on the magnetization distribution in samples and vice versa, problems of positioning the force microscope tip above a surface point under study and so on [3]. In this connection, some other alternative methods of magnetic imaging should be investigated. Among those, the scanning near-field optical microscopy (SNOM) is of a great importance. It combines the rich capabilities of optical methods with the high resolution of scanning probe microscopy [4, 5]. In the SNOM, a probe scans the sample, the distance between them has to be smaller than the wavelength.

The SNOM can be utilized in a variety of different imaging modes including illumination mode, collection mode and dual mode [6, 7]. In all modes, the resolution depends on the aperture size and the probe-sample

spacing rather than on the wavelength. In the illumination mode, the probe acts as an optical near-field generator which illuminates the sample. The signal (transmitted, reflected, or emitted light) is collected in the far-field using conventional optics. In collection SNOM mode, the sample is illuminated using far-field optics and the signal is collected by the SNOM tip. Both illumination mode and collection mode of the SNOM have been utilized and have provided high-resolution imaging [4–9]. The motivation in choosing one imaging mode or another is usually dictated by the particular experiment. The tip can be used also to both illuminate the sample and to collect the signal, a configuration known as dual SNOM mode [10]. This arrangement is attractive because it is easy to implement (there is no need for far-field optics, i.e. the conventional optical microscope). In this mode, however, both the illumination light and the collected signal must pass through the aperture causing significant reduction in the signal-to-noise ratio.

Like conventional optical microscopy, SNOM can be performed in transmission or in reflection geometry. The most common method is the transmission SNOM where a thin, transparent sample is excited by the tip (i.e. illumination mode) and the light signal is collected in the far-field at the opposite side of the sample. For opaque samples, however, the reflection geometry is required. In the reflection SNOM, the tip and collection optics must be placed at the same side of the sample [11, 12].

The first application of the SNOM for the magnetooptical (MO) studies was reported in 1992 [13], when it was demonstrated that near-field MO observation can be obtained in the same manner as conventional far-field observation, i.e., using two crossed polarizers. Betzig et al. [13] visualized magnetic domains of 100 nm size and claimed spatial resolution of 30 to 50 nm. In further works, the possibility of MO domains imaging was confirmed in both transmission regime (Faraday geometry) [14, 15] and in reflection one (Kerr microscopy) [16, 17]. Today, the MO SNOM development is only at the initial stage. The published experimental results are not very numerous and concern mainly to investigation of simple magnetic structures in Co/Pt multilayers [13] and iron-garnet films [14–21]. MO SNOM has indisputable potential for the imaging of magnetic structures due to its high resolution unlimited by the light diffraction. However, some problems arise related to the MO images interpretation. Apart from that, recent experiments on SNOM domains observation in iron-garnet films revealed that high spatial resolution is not always attainable: width of the domain walls (DW) images obtained with the SNOM in [21] is about 0.6 μm, that is, of the same order as for images one can provided by the conventional magnetooptical microscopy.

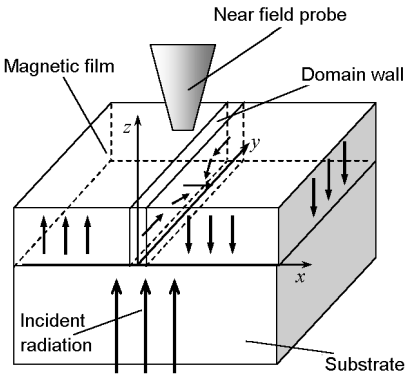

Fig. 1. The structure under investigation.

Further experimental and theoretical work is required to reveal the origin of this phenomenon and to define what is the real spatial resolution of the SNOM depending on particular experiment conditions and what experiment design and sample parameters could assure all the advantages of the near-field imaging. In this paper, we analyze theoretically the SNOM imaging of domain walls in transparent magnetic films.

The theoretical consideration is based on the Green function technique described in [22–25]. Let us consider a semi-infinite transparent substrate with a magnetic film on the surface (Fig. 1). The sample is illuminated by optical wave $\mathbf{E}^{(i)}(\mathbf{r},t) = \mathbf{E}^{(i)}\exp(-i(\mathbf{k}_0\mathbf{r} - \omega t))$.

From the Maxwell equations, we have $rotrot\mathbf{E}(\mathbf{r},t) = -\frac{1}{\varepsilon_0 c^2}\frac{\partial^2}{\partial t^2}\mathbf{D}(\mathbf{r},t)$. Passing to the field complex amplitudes

$$\mathbf{E}(\mathbf{r},t) = \mathbf{E}(\mathbf{r})\exp(i\omega t)$$
$$\text{and } \mathbf{D}(\mathbf{r},t) = \mathbf{D}(\mathbf{r})\exp(i\omega t)$$

in view of the material equation

$$\mathbf{D}(\mathbf{r}) = \varepsilon_0\mathbf{E}(\mathbf{r}) + \mathbf{P}(\mathbf{r})$$

we obtain the equation for **E(r)**

$$rotrot\mathbf{E}(\mathbf{r}) - k_0^2\hat{\varepsilon}(\mathbf{r})\mathbf{E}(\mathbf{r}) = \frac{k_0^2}{\varepsilon_0}\mathbf{P}_1(\mathbf{r}), \quad (1)$$

where $\mathbf{P}_1(\mathbf{r})$ is the part of the medium polarization induced in the magnetic film by the external field and $\varepsilon(\mathbf{r}) =\varepsilon 0,\ z < 0$; $\varepsilon(\mathbf{r}) = 1$, $z > 0$, $\mathbf{P}_1(\mathbf{r}) = \varepsilon_0\chi\mathbf{E}(\mathbf{r})$, χ is the susceptibility of the magnetic film.

In the case under study, the right-hand side of Eg.(1) can be considered as a small perturbation ($P_1 << |\varepsilon_0 E^{(i)}$) and this equation can be solved in the Born first approximation where the field is analytically representable as a sum of two terms:

$$\mathbf{E}(\mathbf{r}) = \mathbf{E}^{(0)}(\mathbf{r}) + \mathbf{E}^{(1)}(\mathbf{r}).$$

Here, $\mathbf{E}^{(1)}(\mathbf{r})$ is the field without the magnetic film which satisfies the homogeneous equation

$$rotrot\mathbf{E}^{(0)}(\mathbf{r}) - k_0^2\varepsilon(\mathbf{r})\mathbf{E}^{(0)}(\mathbf{r}) = 0 \quad (2)$$

and $\mathbf{E}^0(\mathbf{r})$ is the field scattered by the magnetic film which satisfies the inhomogeneous equation

$$rotrot\mathbf{E}^{(1)}(\mathbf{r}) - k_0^2\varepsilon(\mathbf{r})\mathbf{E}^{(1)}(\mathbf{r}) = \frac{k_0^2}{\varepsilon_0}\mathbf{P}_1^{(0)}(\mathbf{r}), \quad (3)$$

where $\mathbf{P}_1{}^0(\mathbf{r})$ is the part of the particle polarization induced by $\mathbf{E}^0(\mathbf{r})$.

Solutions to Eq.(2) are known as Fresnel formulas. Equation (3) is inhomogeneous and can be solved using the Green functions $D_{\mu\nu}(\mathbf{r},\mathbf{r}')$ which are introduced by means of the equation [22]

$$\left(\frac{\partial^2}{\partial x_\lambda \partial x_\mu} - \delta_{\lambda\mu}\frac{\partial^2}{\partial x_\mu^2} - \varepsilon(\mathbf{r})\frac{\omega^2}{c^2}\delta_{\lambda\mu}\right)D_{\mu\nu}(\mathbf{r},\mathbf{r}') = -\delta_{\lambda\nu}\delta(\mathbf{r}-\mathbf{r}') \quad (4)$$

where $\delta_{\lambda\nu}$ is the Kronecker symbol.

The solution to Eq.(3) can be written as

$$E_\mu^{(1)}(\mathbf{r}) = -\frac{k_0^2}{\varepsilon_0}\int D_{\mu\nu}(\mathbf{r},\mathbf{r}')P_{1\nu}^{(0)}(\mathbf{r}')\cdot d\mathbf{r}', \quad (5)$$

where the subscripts μ,ν take the values of x, y, and z. Repeating subscripts imply summation.

The space integration requires a large body of computation. The computation time can be cut in the Fourier space. By introducing the Fourier representations for the Green functions

$$D_{\mu\nu}(\mathbf{r},\mathbf{r}') = \frac{1}{4\pi^2}\int d_{\mu\nu}(\mathbf{k}_\parallel,z,z')\exp\left(i\mathbf{k}_\parallel(\mathbf{r}_\parallel - \mathbf{r}_\parallel')\right)d\mathbf{k}_\parallel,$$

where $\mathbf{r}_\parallel(x,y,0)$, $\mathbf{r}_\parallel'(x',y',0)$ and $\mathbf{k}_\parallel(k_x,k_y,0)$, we can rewrite formula (5) in terms of the Fourier transforms:

$$\hat{E}_\mu^{(1)}(\mathbf{k}_\parallel,z) = -\frac{k_0^2}{\varepsilon_0}\int d_{\mu\nu}(\mathbf{k}_\parallel,z,z')\hat{P}_{1\nu}^{(0)}(\mathbf{k}_\parallel,z')\cdot dz'. \quad (6)$$

Note that the Fourier transforms $d_{\mu\nu}(\mathbf{k}_\parallel, z,z')$ of the Green functions are found by solving ordinary differential equations. The associated procedure is described in [22].

The scattered radiation field can be found by inverse Fourier transformation

$$E_\mu^{(1)}(\mathbf{r}) = \frac{1}{4\pi^2}\int_{\mathbf{k}_\parallel}\hat{E}_\mu^{(1)}(\mathbf{k}_\parallel,\mathbf{r})e^{i\mathbf{k}_\parallel\mathbf{r}_\parallel}d\mathbf{k}_\parallel. \quad (7)$$

We examine here the passive probe model [26] neglecting the probe effect on the SNOM image and assuming that the signal detected is proportional to the near-field intensity at the nanostructure surface in the absence of probe. This assumption may be valid either if the field scattered by the tip is very low or if it is not reflected back by the sample. Thus, from this qualitative analysis, we may expect the probe to be passive either if the tip is very small or if the sample has a low reflectivity. Therefore, a metal tip close to a metal sample may not satisfy the passive probe assumption whereas a tiny metal tip over a dielectric (or magnetic) might be considered as passive probe.

The passive probe model simplifies calculation substantially. Indeed, that approach enables to work in the Born first approximation and to determine the near-field; we only need to calculate the scattered field $\hat{E}_\mu^{(1)}$ $(z, \omega, \mathbf{k}_\parallel)$ by Eq.(6) with $\hat{P}_{1\nu}^{(0)}$ $(z, \omega, \mathbf{k}_\parallel)$ Fourier transform chosen according to the kind of the nanoscaled structure. The specificity of work in the near-field tells on the range of integration $\{\mathbf{k}_\parallel\}$ in Eq.(7). Since the main idea of the SNOM lies in dealing with non-radiation evanescent waves that correspond to the high spatial frequencies, the range $\{\mathbf{k}_\parallel\}$ must include a wide range of $\mathbf{k}_\parallel$, including $\mathbf{k}_\parallel$ for which $|\mathbf{k}_\parallel| > k_0$. The fulfillment of the last inequality is necessary to obtain high spatial resolution. For example, a resolution of 10 nm, that is attainable in the SNOM, can be provided if all spatial harmonics with $k_{x,y} \in (-25k_0, 25k_0)$ are integrated. We should note here that

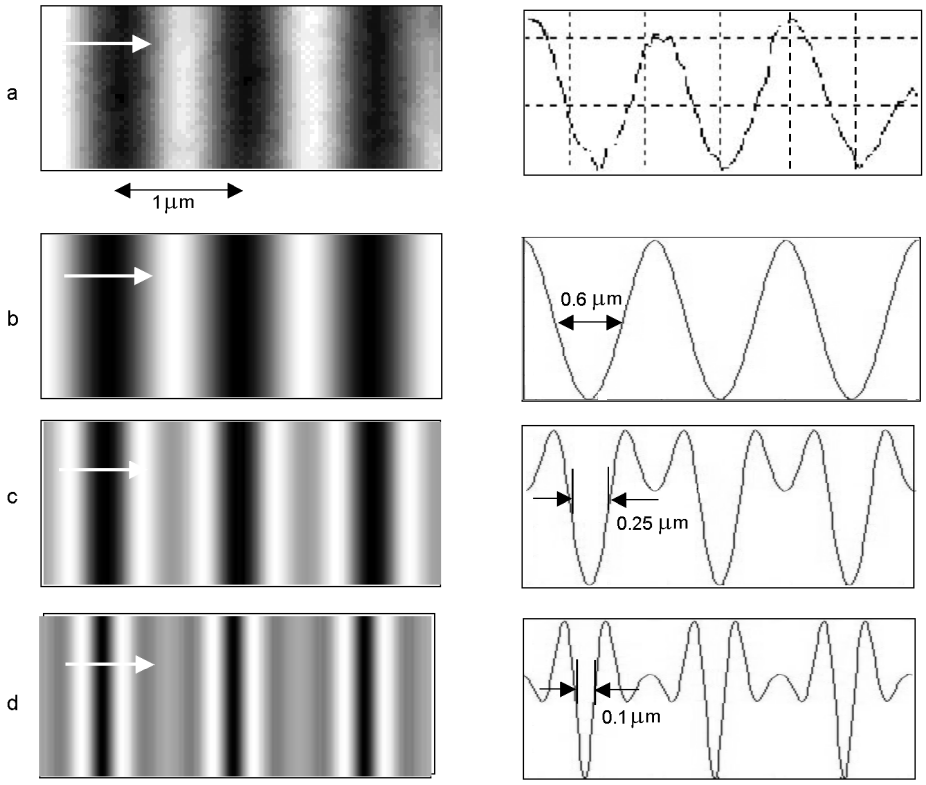

Fig. 2. Experimental (a) and simulated (b–d) SNOM images of the domain structure in magnetic iron-garnet films. Film thickness 7 μm (a), (b), 1 μm (c), 0.1 μm (d). Domain wall width 0.1 μm. Corresponding image intensity cross-sections are presented at each image.

the scanning altitude (z in Eq.(6)) must be not larger than several tens of nanometers.

Let us consider the following model of the magnetization distribution in domains and in DW. To characterize the magnetization direction, we introduce two angles: φ and θ of the standard spherical coordinates with Z axis perpendicular to the magnetic film plane (Fig. 1). For magnetization in the domains, $\theta = 0$ or π (magnetization is parallel and anti-parallel to the Z-axis) and for magnetization in the DW region [27]:

$$\theta(x) = 2\mathrm{arctg}[\exp(\pm \frac{x}{\Delta})],$$

where $\Delta = \sqrt{\frac{A}{K_U}}$, $\varphi(y) = const.$

Δ can be referred to as the DW width. In our calculation, we set it to be 100 nm what is a typical value for samples under investigation. The unit magnetization vector $\mathrm{m} = (m_x, m_y, m_z) = m(\sin\theta\cos\varphi, \sin\theta\sin\varphi, \cos\theta)$. Dielectric susceptibility of the magnetic film is defined as

$$\hat{\chi} = \begin{pmatrix} \varepsilon - 1 & 0 & 0 \\ 0 & \varepsilon - 1 & 0 \\ 0 & 0 & \varepsilon - 1 \end{pmatrix} + ig \begin{pmatrix} 0 & -m_z & m_y \\ m_z & 0 & -m_x \\ -m_y & m_x & 0 \end{pmatrix},$$

where g is the gyration vector [28], $g = 0.01$, $\varepsilon = 4$ (typical values for iron-garnet films).

The calculation results are presented in Fig. 2. In Fig. 2(a), experimental SNOM image of the domain structure in epitaxial iron-garnet films grown on nonmagnetic gadolinium-gallium garnet substrate is shown [21]. The samples had crystallographic orientation <111>. The film thickness was 7 μm, DW width calculated according to [27] is about 0.1 μm, Faraday rotation angle was about 1°/μ. The visible DW width is about 0.6 μm being in a good compliance with the DW width in the respective calculated image (Fig. 2(b)). The other two simulated images correspond to the film thickness 1 μm and 0.1 μm (Fig. 2(c,d)). The actual DW thickness is imaged only in the last case. From the simulated images in Fig. 2 (b)–(d), one can conclude that the DW image width depends on the film thickness: the larger is the thickness,

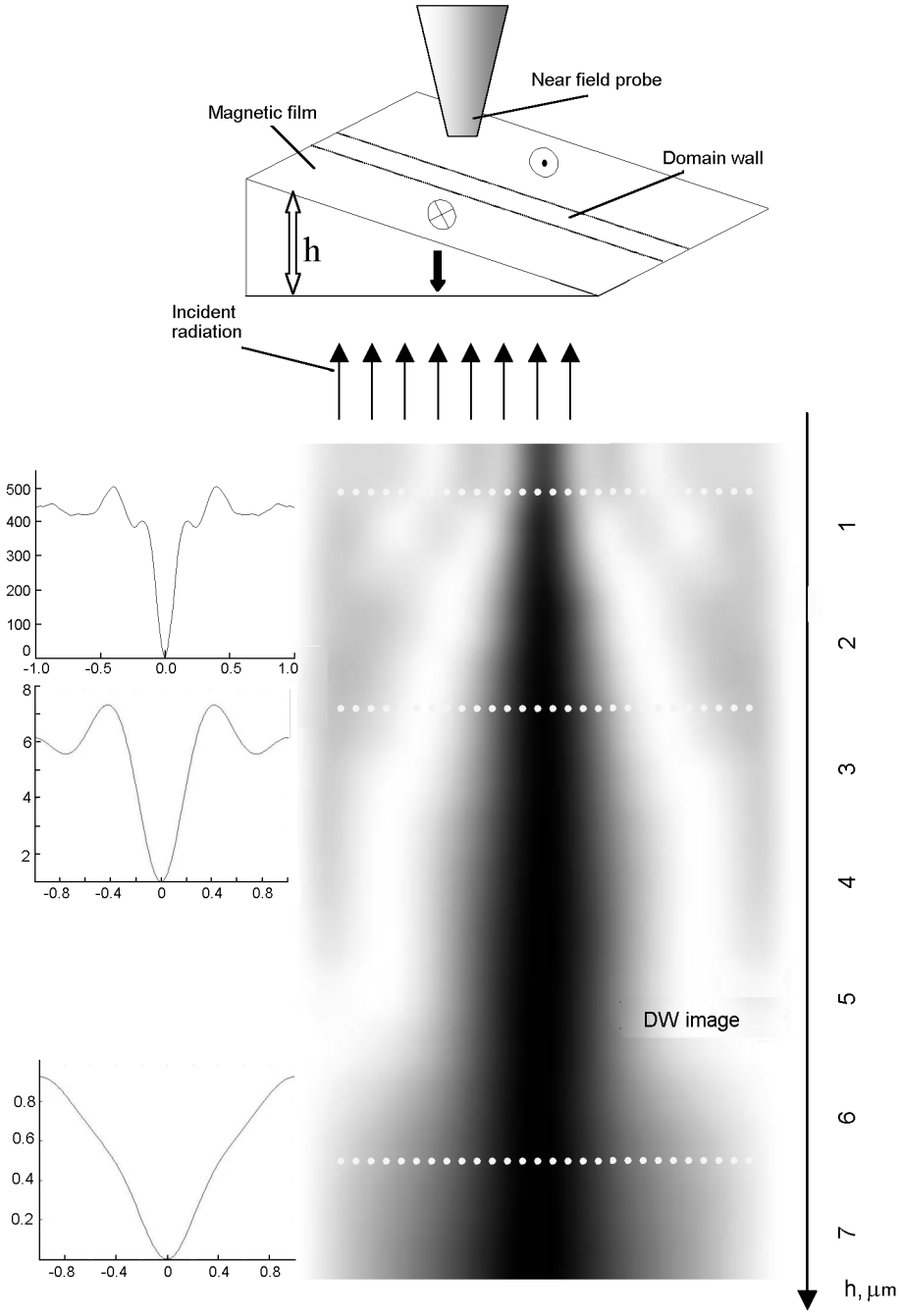

Fig. 3. Simulated image of the 0.1 μm wide domain wall in the wedge-shaped magnetic sample. (a) investigated geometry, (b) domain wall image. Corresponding image intensity cross-sections are presented for three values of the film thickness h.

the wider is the DW image, spatial resolution obtained in SNOM deteriorates with increasing film thickness (note that for all calculations, the wall width in terms of magnetic spin rotation had been set as 100 nm). Thus, the nanometer resolution cannot be attained for thick magnetic films, at least in conventional transmission SNOM geometry. A similar conclusion was also put forward by authors of the theoretical work [29] where a different approach was applied.

Fig. 3 presents simulated image of the DW of constant width $\Delta = 0.1$ μm in a wedge-like shaped magnetic film. This figure is quite demonstrative. Therein, the widening of the DW image with increasing film thickness can be traced.

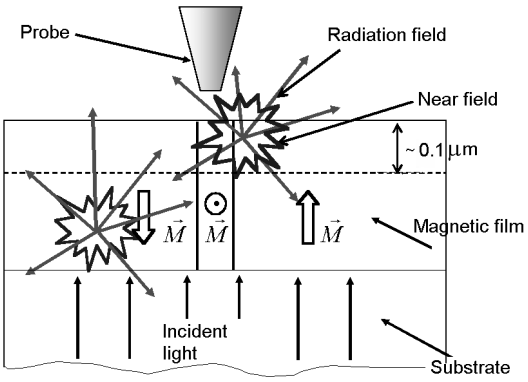

Fig. 4. Radiation and non-radiation (near-field) fields arising in a magnetic film with domain structure. Only near field spatial harmonics radiated from the surface layer of several hundredths of micrometer can attain probe.

The resolution decrease in SNOM for relatively thick magnetic films can be qualitatively explained proceeding from Fig. 4. A very high resolution beyond Relay criterion is attainable due to the presence of evanescent spatial harmonics in detected signal. As the sample thickness increases, the contribution of these evanescent harmonics reduces sharply: the contribution from the film regions located further than several hundred nanometers (for $\lambda = 0.5$ μm) is almost entirely constituted by the far field radiating components that are responsible for low frequency space harmonics and low resolution. So we can conclude that magnetic medium lying below this level does not contribute to the high resolution but only make it worse. Consequently, the best results with transmission SNOM can be achieved only for thin (less than 300 nm thick) films.

Such a limitation for resolution does not exist for reflection measurements because in this case, only thin surface layers contribute into the image. Therefore, SNOM operating in reflection mode is more preferable. However, for the transparent magnetic films reflection signal is weak and one has to search for other configurations in transmission regime. Among such configurations, the aperture-free mode seems to be of good prospects. Thus, further studies are to be conducted in this area.

Thus, the SNOM observation of the domain structure in thick (about 3 to 10 μm) iron-garnet films has been examined. The theoretical analysis was conducted basing on the Green functions method in the Born first approximation (passive probe approach). Simulated SNOM images of domain walls in magnetic films of different thickness revealed resolution dependence on the film thickness. High spatial resolution in transmission aperture SNOM mode is attainable only for comparatively thin films (less than several hundred nanometers). This effect can also be explained on the qualitative level in terms of radiation and evanescent harmonics. The stated theory explains the experimentally observed domain wall image widening in SNOM.

This work is supported by RFBR (№ 01-02-16595, 02-02-17389, 03-02-16980), Federal Program "Russian Universities" 01.03.010/-3.

References

1. Y.Martin, H.K.Wickramasinghe, *Appl. Phys. Lett.*, **50**, 1455 (1987).
2. S.Hosaka, A.Kikukawa, Y.Honda, *Appl. Phys. Lett.*, **65**, 3407 (1994).
3. I.V.Yaminskii, A.M.Tishin, *Usp. Khim.*, **68**, 187 (1999).
4. D.Courjon, C.Bainier, *Rep. Prog. Phys.*, **57**, 989 (1994).
5. D.W.Pohl, *Thin Solid Films*, **264**, 250 (1995).
6. M.Ohtsu, Near Field Nano/Atom Optics and Technology, Springer, Tokyo (1998).
7. G.S.Zhdanov, M.N.Libenson, G.Marcinovskiy, *Physics - Uspekhi*, **41**, 719 (1998).
8. E.Betzig, J.K.Trautman, *Science*, **257**, 189 (1992).
9. M.A.Paesler, P.J.Moyer, Near-Field Optics Theory, Instrumentation and Applications, John Wiley & Sons Inc., New York (1996).
10. D.Courjon, J.M.Vigoureux, M.Spajer et al., *Appl. Opt.*, **29**, 3734 (1990).
11. K.D.Weston, J.A.DeAro, S.K.Buratto, *Rev. Sci. Inst.*, **67**, 2924 (1996).
12. E.Betzig, P.L.Finn, J.S.Weiner, *Appl. Phys. Lett.*, **60**, 2484 (1992).
13. E.Betzig, J.K.Trautman, R.Wolfe et al., *Appl. Phys. Lett.*, **61**, 142 (1992).
14. U.Hartmann, *J. Magn. Magn. Mater.*, **157/158**, 545 (1996).
15. E.Betzig, J.K.Trautman, J.S.Weiner et al., *Appl. Opt.*, **31**, 4563 (1992).
16. T.J.Silva, S.Schultz, *Rev. Sci. Instrum.*, **67**, 715 (1996).
17. P.Fumagalli, A.Rosenberger, G.Eggers et al., *Appl. Phys. Lett.*, **72**, 2803 (1998).
18. G.Eggers, A.Rosenberger, N.Held et al., *Ultramicroscopy*, **71**, 249 (1998).
19. H.Wioland, O.Bergossi, S.Hudlet et al., *Eur. Phys. J. AP.*, **5**, 289 (1999).
20. T.Lacoste, T.Huser, H.Heizelmann, *Z. Phys. B.*, **104**, 183 (1997).

21. A.A.Ezhov, A.S.Logginov, D.A.Muzychenko et al., *Fiz. Metal. Metalloved.*, **92**, 277 (2001).

22. A.A.Maradudin, D.L.Mills, *Phys. Rev. B*, **11**, 1392 (1975).

23. V.I.Belotelov, A.P.Pyatakov, G.G.Musaev et al., *Optics and Spectroscopy*, **91**, 626 (2001).

24. V.I.Belotelov, A.P.Pyatakov, A.K.Zvezdin et al., *Technical Physics*, **48**, 1 (2003).

25. V.A.Kosobukin, *Phys. Solid State*, **35**, 884 (1993).

26. M.Nieto-Vesperinas, J.C.Dainty, Scattering in Volumes and Surfaces, Pergamon Press Madrid (1990).

27. A.P.Malozemoff, J.C.Slonczewski, Magnetic Domain Walls in Bubble Materials, Academic, New York (1979).

28. A.K.Zvezdin, V.A.Kotov, Modern Magneto-Optics and Magneto-Optical Materials, Springer, Philadelphia (1997).

29. A.A.Stashkevich, S.Hudlet, *Opt. Commun.*, **199**, 305 (2001).

Сканувальна ближньо-польова оптична мікроскопія магнітних структур у магнітних плівках

В.І.Бєлотєлов, А.С.Логгінов, А.В.Ніколаєв, А.П.Пятаков, А.К.Звєздін

Магнітооптичне спостереження меж магнітних доменів у плівках залізних гранатів способом ближньо-польової сканувальної оптичної мікроскопії досліджено з точки зору виявлення переваг ближньо-польового зображення стосовно до просторового розрішення. Недавні експерименти показали, що ближньо-польове дослідження доменної структури магнітних плівок товщиною 5–10 мкм не забезпечує істотного підвищення просторового розрішення у порівнянні зі звичайною оптичною мікроскопією. Теоретичний аналіз на основі функцій Гріна показує, що вирішальну роль у цьому ефекті відіграє товщина плівки. Представлено також якісне пояснення погіршення розрішення зі збільшенням товщини плівки.